Band structures of Si_xGe_{1-x} alloys

Srinivasan Krishnamurthy and A. Sher
SRI International, Menlo Park, California 94025

A.-B. Chen
Physics Department, Auburn University, Auburn, Alabama 36849
(Received 16 July 1985)

By starting from realistic band structures of the constituent materials, the electronic structure of Si_xGe_{1-x} alloys are obtained in the coherent-potential approximation (CPA). Various quantities, including the bowing parameter of the fundamental band gap and the energies of several optical gaps, the masses, and the linewidths of the E_0 and E_1 transitions, are calculated on the basis of both diagonal and off-diagonal CPA. All of the band-energy and linewidth predictions are in good agreement with experiments. Furthermore, the theory yields an alloy-scattering-limited electron-drift mobility in qualitative agreement with experimental results.

I. INTRODUCTION

Semiconductor alloys offer the freedom to design material properties by choosing appropriate alloy constituents. In some cases, the physical properties of the alloys can be quite different from those of the constituents.[1-4] In recent years, there has been a renewed interest in Si_xGe_{1-x} alloys[5] and superlattices.[5-10] Because silicon is the most technologically advanced semiconductor, the results on Si-Ge systems have many potential applications.

The lattice constants of silicon and germanium differ by $\sim 4\%$. Hence, the strain introduced in the formation of Si_xGe_{1-x} alloys can affect the band structure[10] and the transport properties.[8] Prior authors used virtual-crystal approximation (VCA) (Refs. 11 and 12) and coherent-potential approximation (CPA) (Ref. 13) to study the band structure and related properties. Either because of less accurate band structures of the constituent materials, or because of the approximations involved in the alloy formalism, these calculations predicted only trends of specific quantities, not quantitatively accurate results. Because the s-state site potentials (ϵ_s) for silicon and germanium differ by approximately 1.5 eV, VCA cannot accurately describe effective masses and other finer details of the band structure. Because of the use of poor basis functions, earlier CPA work[13] predicted alloy broadening of conduction-band states substantially differing from experiment. The purpose of this paper is to correct these flaws and treat transport phenomena.

Because of a substantial difference between the site potentials and lattice constants of silicon and germanium, we incorporated both chemical and structural disorder in the calculation of the electronic structure of Si_xGe_{1-x} alloys. Thus, both diagonal and off-diagonal CPA are included in the predicted band structure and related quantities. Parts of the band structure have been used to study the Si $2p$ core exciton[14] and the alloy mobilities.[15] A comprehensive report of the calculations and results is presented here.

The rest of the paper is arranged as follows. The detailed procedure of fitting silicon and germanium band structures is given in Sec. II. The VCA, CPA, and off-diagonal CPA calculations are described in Sec. III. The results and interpretation of the alloy band structures and mobility are given in Sec. IV.

II. BAND-STRUCTURE BASIS

In order to derive an accurate alloy band structure, one must start from a realistic band structure of the constituent materials. Chen and Sher have developed a method,[16] following a prescription of Kane[17] and Chadi,[18] which includes all long-range interactions, and then they have fine-tuned the band structure with an adjustable local Hamiltonian. Because the details have already been published,[16,19] the underlying method will be presented here in brief.

Gaussian orbitals of the type α (α can be s, p_x, p_y, or p_z) for each sublattice in a cell are used to construct the corresponding Bloch basis. In this basis set, the overlap matrix and the Hamiltonian derived from empirical pseudopotentials can be calculated.[17,18] It is possible to cast the problem in a basis set of Gaussian orbitals in which, in crystal units (c.u.), the same exponential factors apply for all III-V compounds.[19] In this universal basis, the overlap matrix and the kinetic energy matrix are the same for all III-V compounds. Then, by a unitary transformation, the basis set is orthonormalized.[20] The Hamiltonian in this new basis set denoted $H_0(\mathbf{k})$. The band structure resulting from this method reproduces the results of elaborate band-structure calculations within a few percent throughout the Brillouin zone (BZ). To establish accurately certain important band-structure features adjacent to the gap, an extra small 8×8 Hamiltonian matrix $H_1(\mathbf{k})$ is added to $H_0(\mathbf{k})$. This $H_1(\mathbf{k})$ has the form of a tight-binding (TB) Hamiltonian, in which only the nearest-neighbor interactions are included, and simulates the effect of nonlocal pseudopotentials and an expanded orbital set. The total Hamiltonian $H(\mathbf{k})$ in this orthonormalized basis set is diagonalized to obtain the band ener-

gies and the corresponding wave functions.

Following this procedure with the same exponential factor $\beta=0.26$ in the Gaussian orbitals for both silicon and germanium, the matrix $H_0(\mathbf{k})$ is obtained. For silicon and germanium, H_1 contains six adjustable parameters: namely, the corrections to the term values Δ_s and Δ_p and to the nearest-neighbor interactions V_{ss}, V_{sp}, V_{xx}, and V_{xy}. The values of Δ_s, Δ_p, V_{ss}, and V_{xx} are determined from fitting the three experimental energy gaps[21–28,39] at $\Gamma(\mathbf{k}=0)$: Γ_2'-Γ_1, Γ_{15}- Γ_{25}', and Γ_2'- Γ_{25}', and the photoelectric threshold values -5.07 and -4.80 eV for silicon and germanium, respectively.[29] The remaining parameters V_{sp} and V_{xy} are obtained from the experimental values[21–28] of the gaps X_{1c}-X_{1v} and L_{1c}-L_{3v}'. Some adjustments in these input quantities are made to obtain an overall good band structure with more accurate effective masses. Table I lists the empirical pseudopotential form factors and the parameters used to obtain the band structure. The calculated band structures and experimental values are given in Table II. From Table II, one can see that an excellent fit to the silicon and germanium band structure is obtained: All the calculated values lie within the experimental uncertainties. The optical difference between L_{1c} and L_{3v}, Γ_{25}' and Γ_{15} are in excellent agreement with the known optical transition values.

Although the calculated effective transverse masses agree very well with experiment, the effective longitudinal mass for germanium is less than the experimental value. This is due mainly to our attempt to have a common β and the choice of local pseudopotentials, causing $H_0(\mathbf{k})$ to be the same in crystal units (c.u.) for both germanium and silicon. Because of the common $H_0(\mathbf{k})$, the alloy disorder is contained in these adjusted parameters. This H_0 would also be useful for the interface and superlattice[31] problems. If we grant ourselves the freedom to adjust V_{xy}, longitudinal effective mass in germanium can be fitted to the experimental value. When V_{xy} is changed, the L_{1c},L_{3v}' will also change. We have chosen not to do this because little is gained for the extra complexity. For an indirect-gap semiconductor, the important effective mass used in transport studies is the conductivity mass

$$3(1/m_{el}^*+2/m_{et}^*)^{-1}\ .$$

Because $m_{el}^* \gg m_{et}^*$ in germanium, m_c^* will not be much different if a less accurate value of m_{et}^* is used. Moreover, the Si_xGe_{1-x} alloys which have potential device applications are in the silicon-rich region, where the effective mass at the L edge is not expected to affect the further studies.

It is important to note that an excellent fit to the experimental values can be obtained with only seven adjustable parameters $(\beta,\Delta_s,\Delta_p,V_{ss},V_{sp},V_{xx},V_{xy})$, with β being universal in c.u. The calculated band structure of silicon and germanium are shown in Fig. 1(a) and 1(b), respectively. The characteristic indirect gaps are clearly seen.

TABLE I. Pseudopotential form factors and the band parameters (in eV).

Parameter	Silicon	Germanium
$V(\sqrt{3})$	−2.872	−2.872
$V(\sqrt{4})$	0.124	0.124
$V(\sqrt{8})$	0.638	0.638
$V(\sqrt{11})$	0.109	0.109
Δ_s	−16.175	−16.922
Δ_p	−16.109	−14.971
V_{ss}	−0.111	0.131
V_{sp}	0.040	0.150
V_{xx}	0.025	0.030
V_{xy}	0.050	0.100

TABLE II. Calculated symmetry-point band energies of silicon and germanium compared with experiments and empirical-pseudopotential-method (EPM) results. (all energies in eV).

	Silicon		Germanium	
Bands	Calculated	Expt.[a]-EPM[b]	Calculated	Expt.[a]-EPM[b]
Γ_1	−12.60	12.4±0.6	−12.56	−12.6±0.3
L_{2v}	−10.26	−9.3±0.4	−10.74	−10.6±0.5
L_{1v}	−6.99	−6.8±0.2	−7.65	−7.4±0.3
X_{1v}	−8.29	−7.69	−9.20	−8.65
X_{4v}	−2.55	−2.86	−2.55	−3.29
L_{3v}'	−1.11	−1.2±0.2	−1.13	−1.1±0.2
Γ_{25v}	0.0	0.0	0.0	0.0
L_{1c}	2.24	2.23	0.76	0.76
Γ_{2c}'	4.10	4.00±0.05	0.99	0.99
Γ_{15c}	3.43	3.40	3.24	3.22
X_{1c}	1.34	1.17	0.95	1.16
L_{3c}'	4.34	4.34	4.16	4.25
E_g	1.11	1.11	0.76	0.76
K_0	(0.8,0,0)	(0.8,0,0)	(0.5,0.5,0.5)	(0.5,0.5,0.5)
m_{el}^*	0.89	0.91	1.09	1.59
m_{et}^*	0.16	0.19	0.077	0.082
m_v^*	0.35	0.50	0.28	0.34

[a]References 21–28.
[b]Reference 30.

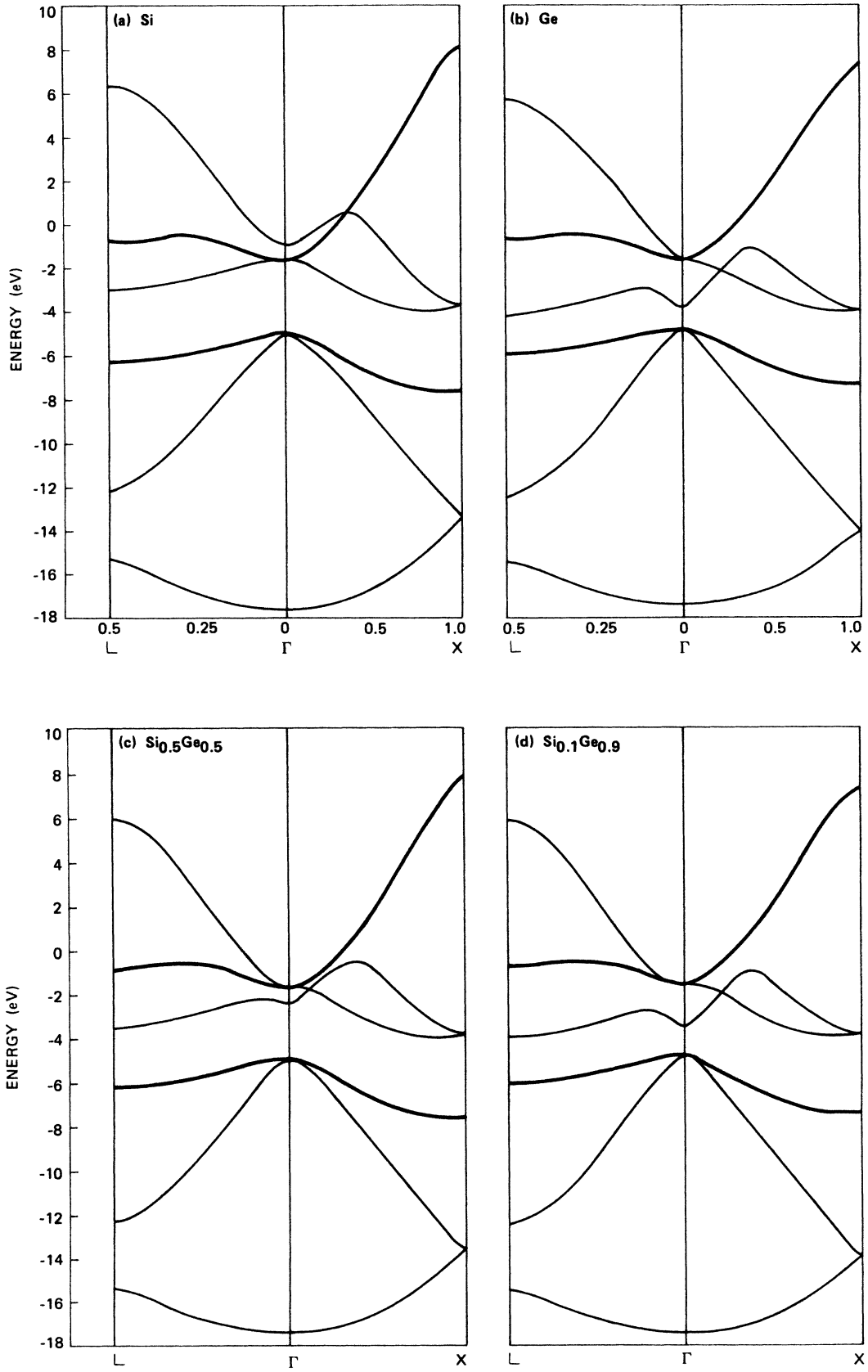

FIG. 1. Calculated VCA band structures of (a) silicon, (b) germanium, (c) $Si_{0.5}Ge_{0.5}$ alloys, and (d) $Si_{0.10}Ge_{0.90}$. (e) (Shown on facing page) shows calculated VCA values (solid) and the experimental values (dashed) of the E_0 and E_0' peak positions plotted as a function of alloy concentration x.

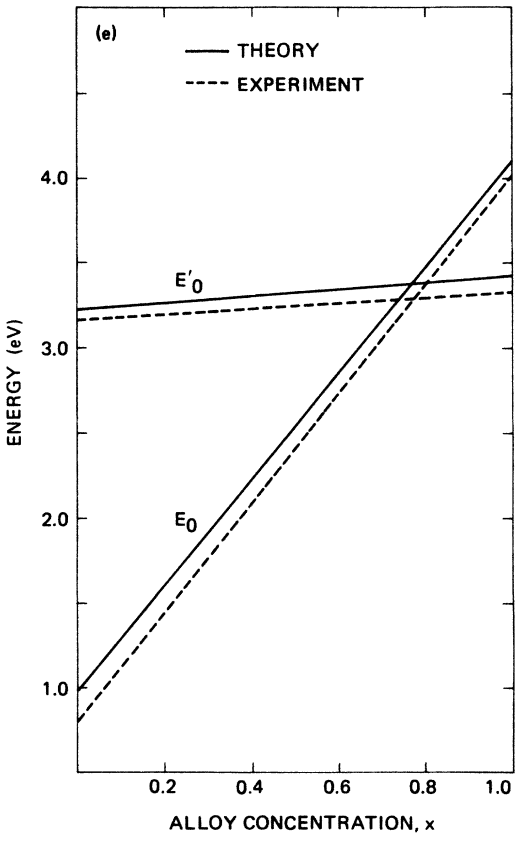

FIG. 1. *(Continued).*

These band structures compare favorably with the best results available, and, in contrast with those obtained in the usual empirical TB approaches, produce good conduction bands. However, if they were included, the spin-orbit interactions (neglected in this work) would add some fine details, especially the splitting between the heavy- and light-hole bands near Γ.

III. ALLOY CALCULATION

A. VCA

Because we have the same $H_0(\mathbf{k})$ matrix for both silicon and germanium, it is only the H_1 matrices of the constituents in scaled VCA which distinguishes them. In this approximation, the diagonal elements of the alloy Hamiltonian $\overline{H}(\mathbf{k})$ are simply the concentration-weighted average of the corresponding elements of the pure silicon and germanium Hamiltonians, whereas the off-diagonal elements of $\overline{H}(\mathbf{k})$ are obtained by assuming a $1/d^2$ dependence. $\overline{H}(\mathbf{k})$ can be diagonalized to obtain the VCA band structure for various concentrations x. The VCA band structures for $x=0.1$ and 0.5 are shown in Fig. 1(c) and 1(d), respectively.

B. Diagonal CPA

An earlier work on CPA band structure of SiGe alloys[13] is based on a local but energy-dependent pseudopotential approximation. While the value of the principal scattering potential parameter, the difference between the s-electron site potentials in Si and Ge, was 1.49 eV, close to our value 1.46 eV, the calculation predicted too-large linewidths in the E_0 spectrum and essentially no effect on the electron mobility. With the availability of a set of good basis functions and constituent band structures, more realistic band structures of the alloy can be obtained.

In the current model, we have a TB Hamiltonian, which contains matrix elements to all ranges. The simplest alloy model is to assume that the important disorder resides only in the diagonal matrix elements ϵ_s and ϵ_p. In our model, the ϵ_s^{Si} and ϵ_s^{Ge} differ by 1.46 eV, whereas ϵ_p^{Si} and ϵ_p^{Ge} differ by 0.21 eV. For the present, we neglect the disorder in the off-diagonal element. Mathematically, we have

$$H_{\mathrm{alloy}}=\overline{H}+\sum_l V_l\ , \tag{1}$$

where l is a fcc lattice vector identifying a site, and V_l is the 8×8 diagonal matrix with elements $U_s=\epsilon_s-\overline{\epsilon}_s$, $U_p=\epsilon_p-\overline{\epsilon}_p$ in the orthonormal local orbital $\mathrm{s}\,|\,lj\alpha\rangle$; j denotes the two atoms in the unit cell labeled l, α represents s or p symmetry, and $\overline{\epsilon}_s$ and $\overline{\epsilon}_p$ are the concentration-weighted average values of s and p silicon and germanium term value energies.

The one-particle alloy Green's function is defined as

$$G_{\mathrm{alloy}}(Z)=\frac{1}{Z-H_{\mathrm{alloy}}}\ . \tag{2}$$

We are after the configuration average of this Green's function, which, in effective medium theory, is replaced by an effective Green's function G,

$$G(Z)=\frac{1}{Z-\overline{H}-\Sigma(Z)}\ , \tag{3}$$

where Σ is the self-energy. In CPA, we can now write $\Sigma=\sum_l(\Sigma_l)$, with Σ_l being an 8×8 matrix in the basis $|\,lj\alpha\rangle$ having the form

$$\underline{\Sigma}=\begin{bmatrix}\underline{A} & \underline{0}\\ \underline{0} & \underline{A}\end{bmatrix}\ , \tag{4}$$

where

$$\underline{A}=\begin{bmatrix}\Sigma_s & 0 & 0 & 0\\ 0 & \Sigma_p & 0 & 0\\ 0 & 0 & \Sigma_p & 0\\ 0 & 0 & 0 & \Sigma_p\end{bmatrix}\ .$$

Here Σ_s and Σ_p are the s and p parts of the self-energy. The Σ_s and Σ_p are determined from the conditions that the average atomic t matrix with respect to the CPA Green's function G is zero. With our ansatz for Σ, the matrix equation $\langle t\rangle=0$ reduces to two coupled equations $\langle t_s\rangle=0$ and $\langle t_p\rangle=0$, where the average is the concentration-weighted average $\langle Q\rangle=xQ^{\mathrm{Si}}+yQ^{\mathrm{Ge}}$, and the t is defined as

$$t_\alpha^\beta=(U_\alpha^\beta-\Sigma_\alpha)[1-F_\alpha(U_\alpha^\beta-\Sigma_\alpha)]^{-1}\ ,$$

$$(\alpha=s\text{ or }p\ ,\ \beta=\mathrm{Si}\text{ or Ge})\ . \tag{5}$$

In the above expression F_α is the diagonal matrix element of G in the local basis

$$F_\alpha(Z)\equiv\langle lj\alpha\,|\,G(Z)\,|\,lj\alpha\rangle\ .$$

Σ_s and Σ_p are coupled because F_s and F_p each contain both Σ_s and Σ_p.

An iterative average-t-matrix (IATA) procedure[19] is employed to solve the CPA equation. This procedure improves Σ_α upon a guessed solution Σ_α^0 through the following equations:

$$\begin{aligned}\Sigma_s&=\Sigma_s^0+\langle t_s^0\rangle(1+F_s^0\langle t_s^0\rangle)^{-1}\ ,\\ \Sigma_p&=\Sigma_p^0+\langle t_p^0\rangle(1+F_p^0\langle t_p^0\rangle)^{-1}\ ,\end{aligned}\tag{6}$$

where $\langle t_\alpha^0\rangle$ and F_α^0 are similar to those in Eq. (5) except that Σ_α^0 now replaces Σ_α. The most time-consuming calculation is then the computation of the local Green's functions F_s^0 and F_p^0, given by the BZ summation, e.g.,

$$F_s^0(Z)=\frac{1}{N}\sum_{\mathbf{k}}\left[\frac{1}{Z-\bar{H}(\mathbf{k})-\Sigma_s^0}\right]_{11}\ ,$$

where the inverse of an 8×8 matrix is involved for every $\mathbf{k}$. This can be simplified by observing that Σ_α^0 has the same form as Σ in Eqs. (4) and (5) and that the 4×4 $\underline{A}$ matrix can be written as $\underline{A}=\Sigma_p\underline{1}+(\Sigma_s-\Sigma_p)\underline{J}$, where $\underline{1}$ is the identity matrix and

$$\underline{J}=\begin{bmatrix}1&0&0&0\\0&0&0&0\\0&0&0&0\\0&0&0&0\end{bmatrix}\ .$$

Defining the matrix

$$\underline{\sigma}=(\Sigma_s^0-\Sigma_p^0)\begin{bmatrix}\underline{J}&\underline{0}\\\underline{0}&\underline{J}\end{bmatrix}\ ,$$

$F_s^0(Z)$ and $F_p^0(Z)$ can now be calculated from

$$\begin{aligned}F_s^0(Z)&=\frac{1}{N}\sum_{\mathbf{k}}g_{11}(\mathbf{k},Z)\ ,\\ F_p^0(Z)&=\frac{1}{3N}\sum_{\mathbf{k}}[g_{22}(\mathbf{k},Z)+g_{33}(\mathbf{k},Z)+g_{44}(\mathbf{k},Z)]\ ,\end{aligned}\tag{7}$$

where

$$g=g^0+g^0(1-\sigma g^0)^{-1}\ ,\tag{8}$$

with

$$g_{\alpha\beta}^{(0)}(\mathbf{k},Z)=\sum_n\frac{U_{n\alpha}^*(\mathbf{k})U_{n\beta}(\mathbf{k})}{Z-\epsilon_n(\mathbf{k})-\Sigma_p^0}\ .\tag{9}$$

In Eq. (9), $\epsilon_n(\mathbf{k})$ is the band energy in VCA and $\{U_{\alpha n}(\mathbf{k})\}$ satisfy the following Eigen equation:

$$\sum_\beta\bar{H}_{\alpha\beta}(\mathbf{k})U_{\beta n}(\mathbf{k})=\epsilon_n(\mathbf{k})U_{\alpha n}(\mathbf{k})\ .$$

Because the σ matrix has only two nonzero elements, the matrix inversion in Eq. (8) is obtained analytically.

A substantial reduction in computer time is made possible by using an analytical continuation method.[32] In this method, Σ_s and Σ_p are calculated as a function of complex Z, and then, using the analytical properties of the self-energy and Green's functions, they are interpolated for real Z. Because the functions Σ_s, Σ_p, and G are smooth for complex Z, the CPA iterations and BZ integrations can be carried out with substantially less computer time.

For the concentrations $x=0.10$ and 0.50, the L and X (Δ) gaps, respectively, are preferred. The L to X (Δ) crossover takes place near $x\approx0.15$. The CPA correction to L and X edges at $x=0.10$, 0.15, and 0.50 should be good enough to study the quantitative variation of band gap in Si_xGe_{1-x} alloys. Hence, the calculations are carried out for these three cases. In addition, because the experimental results are available for $x=0.109$, CPA calculations are also done here for comparison. As expected, Σ_s is much larger than Σ_p for all the cases. The self-energy as a function of energy is plotted in Fig. 2 for an $x=0.50$ alloy.

C. Off-diagonal CPA

As mentioned earlier, silicon and germanium differ in their lattice constant by $\sim4\%$. In order to include the effect of the structural disorder, the CPA calculation is repeated next with off-diagonal (OD) disorder included. By an application of the molecular coherent-potential approximation (MCPA),[33] Hass *et al.* included OD disorder in the CPA calculation of $A'_xA''_{1-x}B$ semiconductor alloys.[34] Assuming that B atoms occupy the sites of an ordered zinc-blende virtual lattice, they modeled the dominant structural effect as the difference in A'-B and A''-B hopping matrix elements. Hence, the chemical and structural disorder effects are treated as random variations of $\epsilon^A, V_1^A, V_2^{AB}$, where the symbols have their usual meaning.[35]

The extension of the method to Si_xGe_{1-x} alloys is not straightforward, mainly because silicon and germanium can occupy both sublattices; hence, there can be no ordered virtual lattice in this case. If we choose the tetrahedral unit cell as the molecular unit for MCPA, we see that the disorder is not cell diagonal. However, by choosing an appropriate basis set, we can make the intercell interaction be the highest-order effect. We start with a hybrid basis $|lh\rangle_i$ obtained from the sp^3 hybrid orbitals.[35] The hybrids 1 through 4 ($i=1$–4) are obtained from orbitals centered on a sublattice I site, and the states 5 through 8 ($i=5$–8) are those from the orbitals located at the four nearest-neighbor sites on sublattice II. The Bloch basis states, corresponding to A_1, T_2 symmetries, $|\mathbf{k}\rangle_i$ located on a I site ($i=1$–4) and II site ($i=5$–8), are obtained from the corresponding hybrid states given by the relation

$$|l\rangle_i=\sum_{j=1}^{8}C_{ij}\,|lh\rangle_j\ ,\tag{10}$$

where

$$\underline{C}=\begin{bmatrix}\underline{c}_1&\underline{0}\\\underline{0}&\underline{c}_1\end{bmatrix}$$

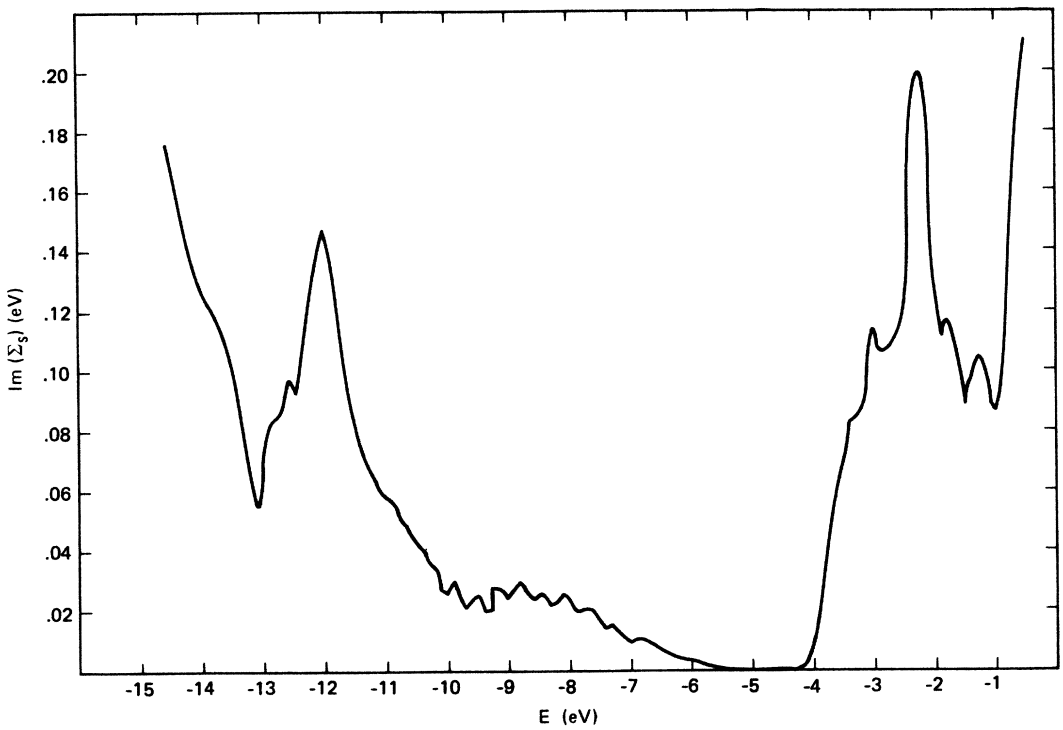

FIG. 2. Variation of the imaginary part of the self-energy Σ_s(CPA) as a function of energy for $x=0.50$.

and

$$\underline{c}_1=\frac{1}{2}\begin{bmatrix}1&1&1&1\\1&1&-1&-1\\1&-1&1&-1\\1&-1&-1&1\end{bmatrix}.$$

An explicit definition of these orbitals can be found in Ref. 20. In this new basis, the self-energy Σ at the given site takes the form

$$\underline{\Sigma}=\begin{bmatrix}\underline{\sigma}_0&\underline{\sigma}_2\\\underline{\sigma}_2&\underline{\sigma}_0'\end{bmatrix}, \tag{11}$$

where

$$\underline{\sigma}_0=\begin{bmatrix}\Sigma_s&0&0&0\\0&\Sigma_p&0&0\\0&0&\Sigma_p&0\\0&0&0&\Sigma_p\end{bmatrix},$$

$$\underline{\sigma}_2=\begin{bmatrix}\Sigma_s'&0&0&0\\0&\Sigma_p'&0&0\\0&0&\Sigma_p'&0\\0&0&0&\Sigma_p'\end{bmatrix}, \tag{12}$$

$$\underline{\sigma}_0'=\begin{bmatrix}\Sigma_h'&0&0&0\\0&\Sigma_h'&0&0\\0&0&\Sigma_h'&0\\0&0&0&\Sigma_h'\end{bmatrix},$$

and

$$\Sigma_h'=\tfrac{1}{4}(3\Sigma_p+\Sigma_s), \tag{13}$$

where $(\Sigma_s,\Sigma_p),(\Sigma_s',\Sigma_p')$ are, respectively, the self-energies associated with diagonal and off-diagonal disorder corresponding s and p symmetries.

The self-energies can be obtained again from the IATA iteration procedure:

$$\Sigma=\Sigma_0+\langle\langle T\rangle\rangle(1+F\langle\langle T\rangle\rangle)^{-1}, \tag{14}$$

where

$$F_{ij}=\frac{1}{N}\sum_n\sum_{\mathbf{k}}\frac{Q_{in}^{\dagger}Q_{nj}}{Z-E_n(Z,\mathbf{k})}, \tag{15}$$

with

$$[\overline{H}(\mathbf{k})+\Sigma]Q=E(Z,\mathbf{k})Q,$$
$$\langle\langle T\rangle\rangle=x\langle T_A\rangle+y\langle T_B\rangle,$$

and

$$\langle T_A\rangle=x^4t_{A_4}^A+4x^3yt_{A_3B}^A+6x^2y^2t_{A_2B_2}^A+4y^3xt_{AB_3}^A+y^4t_{B_4}^A,\quad A\equiv\text{Si} \tag{16}$$

with a similar expression for $\langle T_B\rangle$. Physically, for a given A atom at the center, the other four atoms in the molecular unit cell can be all A atoms, three A atoms and one B atom, two of each, one A atom and three B atoms, or all four can be B atoms. $\langle T_A\rangle$ or $\langle T_B\rangle$ represents the configuration-averaged t matrices, and $\langle\langle T\rangle\rangle$ is the concentration-weighted average of the configuration. By exploiting the symmetry, as seen in Eq. (11), one can

reduce this problem to solving two 2×2 coupled matrix equations. Equation (14) can be iterated to obtain Σ_s, Σ_p, Σ_s', and Σ_p'. After every iteration, we get a new set of Σ_s, Σ_p, Σ_s', Σ_p', and Σ_h': The new set has not been tested to see if Σ_h' is still given by Eq. (13). In our calculation, we did not iterate to obtain a new Σ_h'; the error introduced by this approximation is expected to be very small. As in the case of diagonal CPA, the computation can be substantially reduced by the method of analytical continuation.[32]

IV. DISCUSSION

A. E_0 and E_1 optical transitions

The VCA values of E_0 (Γ_{2c}'-Γ_{25v}) and E_0' (Γ_{15c}-Γ_{25v}) and their measured values are plotted as a function of x in Fig. 1(e). Because the measurements[36] are made at room temperature, the experimental values are smaller than the values calculated from the zero-temperature band structure. Inclusion of the relativistic effects, which are not present in our calculations, is expected to form a more accurate basis for comparison with the experiments. As seen from Fig. 1(e), the theoretical and the experimental values both have a linear variation with x. Similar calculations of E_1 ($L_{1c}-L_{3v}'$) also have a linear variation on x and are in qualitative agreement with experiments.[36]

From the CPA self-energies Σ_s and Σ_p, it is straightforward to calculate the correction to the VCA bands. The calculated complex band structure is plotted for $x=0.50$ in Fig. 3. The CPA corrections are shown only in the vicinity of the band gap. The shaded portion represents the half-width of that energy state. Because s scattering is dominant in these alloys, we see that the major disorder lies in the conduction band. The topmost valence band, with its rich p content, is least affected. The CPA band structure is used to calculate the E_0 and E_1 peak positions for $x=0.10$, 0.109, 0.15, and 0.50 concentrations. The calculations and the data from Ref. 36 show a small bowing that is not seen on the scale of Fig. 1(e).

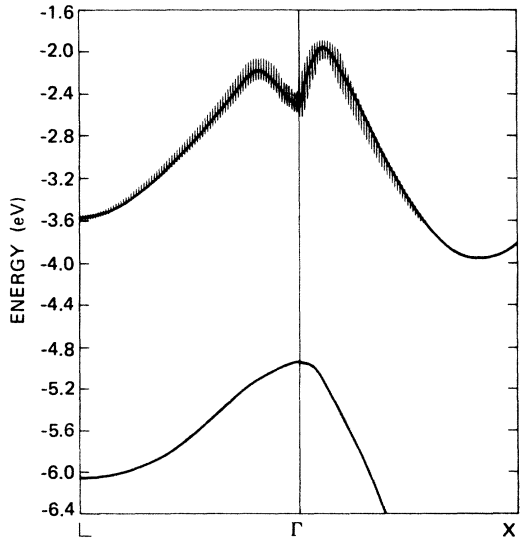

FIG. 3. Calculated CPA complex band structure of the $Si_{0.5}Ge_{0.5}$ alloy. Only the bands in the vicinity of the energy gap are shown. The shaded portion represents the alloy broadening.

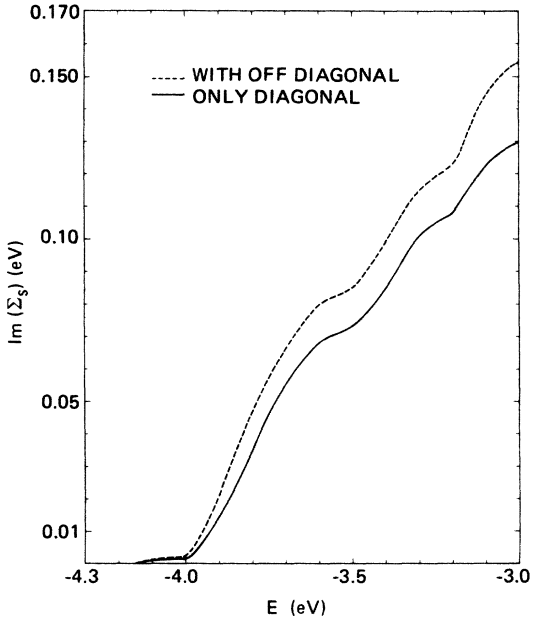

FIG. 4. Imaginary part of Σ_s(CPA) and Σ_s(MCPA) as a function of energy for $x=0.50$ alloy.

The self-energies Σ_s, Σ_p, Σ_p', and Σ_s' are calculated in MCPA for the $x=0.50$ alloy. As in the case of CPA, the self-energies associated with s symmetry are much larger than the ones associated with the p symmetry. While Σ_s' is found to be very small, Σ_p' is at least an order of magnitude smaller—almost zero. However, the $\mathrm{Im}\Sigma_s$ obtained by CPA and MCPA differ considerably. As seen from Fig. 4, the difference increases as one goes away from the band edge. Therefore, the lifetime associated with the alloy disorder is decreased by the inclusion of OD structural disorder. In addition, the OD disorder lowers the conduction band, introducing an extra bowing. The E_0 and E_1

TABLE III. Calculated values of E_0,E_1 and their respective half-widths $\Delta(E_0)$ and $\Delta(E_1)$ (all energies are in eV).

X	Quantity	VCA	CPA	MCPA
0.10	E_0	1.290	1.248	
	$\Delta(E_0)$		0.011	
	E_1	2.016	1.995	
	$\Delta(E_0)$		0.001	
0.109	E_0	2.028	2.009	
	$\Delta(E_0)$		0.013	
	E_1	1.318	1.275	
	$\Delta(E_1)$		0.002	
0.15	E_0	1.442	1.382	
	$\Delta(E_0)$		0.032	
	E_1	2.083	2.051	
	$\Delta(E_1)$		0.002	
0.50	E_0	2.517	2.418	2.391
	$\Delta(E_0)$		0.186	0.206
	E_1	2.578	2.510	2.498
	$\Delta(E_1)$		0.0308	0.0319

values are reduced by 27 and 12 meV, respectively. The VCA, CPA, and MCPA values of E_0 and E_1 are listed in Table III.

The half-width of the alloy states is calculated from the imaginary part of the CPA self-energies. The half-width of the lowest-lying conduction band of $Si_{0.5}Ge_{0.5}$ alloy is plotted in Fig. 5 as a function of K_x in the [100] direction. The calculated half-width is 186 meV for the Γ_2' state and decreases to zero at the band edge. Because of the negligible alloy broadening of the topmost valence-band state, the half-width corresponding to the E_0 transition, $\Delta(E_0)$, is 186 meV, which is approximately one-half of the previously published CPA results.[13] The CPA value of the half-width corresponding to the E_1 transition, $\Delta(E_1)$, is 31 meV. Because of the increase in the imaginary part of the self-energies, the MCPA values of the half-widths of the E_0 and E_1 transitions are 206 and 32 meV, respectively. Because the complete E_0 peak is not shown in the published electroreflectance spectrum,[36] it is difficult to estimate the corresponding half-width. However, one can conclude from the spectrum of the $x=0.458$ alloy that the half-width of the E_1 transition is considerably smaller ($\simeq$50 meV) than that of the E_0 transition. The agreement between the experimental and the theoretical values can be regarded as good because there are errors in estimating the width from the published spectra, and we have neglected the extrinsic broadening due to the apparatus used in the experiments.

In order to make a more accurate comparison with the experiments, the CPA values of $\Delta(E_0)$ and $\Delta(E_1)$ are calculated for the $x=0.109$ alloy. The calculated half-widths of the E_0 and E_1 transitions are 13 and 2 meV, respectively. From the spectrum, we estimate the corresponding values to be 8–15 and 3–6 meV. We see that CPA values are in excellent agreement with these experiments. Because x is small, the inclusion of off-diagonal disorder is not expected to change the calculated values significantly.

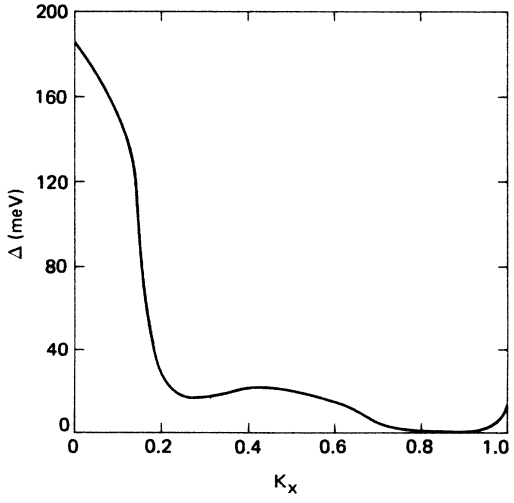

FIG. 5. Variation in the width of the lowest-lying conduction band as a function of K_x in the [100] direction for the $x=0.50$ alloy.

B. Energy gap

The fundamental gaps of these alloys are calculated as a function of concentration. The VCA gap is an increasing function of x with a slope discontinuity at $x\simeq 0.11$. The conduction-band minimum changes from L point to X (Δ) point at this crossover. In addition to the band gap, the effective electron masses and the band edge K_0 are also calculated. When X (Δ) gap is preferred, the band edge moves linearly from $\mathbf{k}$ at $(0.9,0,0)_{x=0.15}$ to $(0.8,0,0)_{x=1}$. The effective masses at a given minimum increase linearly from their pure germanium values to the corresponding pure silicon values.

Using CPA self-energies, the band gap, band masses, and the band edge are also calculated. The position of the band minimum did not change by virtue of the inclusion of off-diagonal disorder. While the effective transverse mass remains almost the same as the VCA value, the longitudinal mass has a maximum of 12% enhancement. Because the real part of CPA self-energies is negative in the forbidden gap region, an extra bowing is introduced to the VCA energy gap. Because of this bowing, the L-X (Δ) crossover takes place near $x\simeq 0.13$. The VCA, CPA, and experimental[36] bowing parameters are 0.06, 0.18, and 0.24, respectively. The calculated energy gap is plotted as a function of x in Fig. 6.

Because of the negligible change in the effective masses, the corresponding values in the pure materials are used in the calculation of the alloy-scattering-limited electron mobility. The CPA X-gap E_g^X and L-gap E_g^L are fitted to a polynomial form. The generalized Brooks's formula that is applicable to the alloys with an indirect gap and multiple bands is used.[15] The calculated electron-drift mobility and the experimental Hall mobility[1] are plotted in Fig. 7, where the theory explains the qualitative behavior of experimental results.[1] As observed,[5] even a few atomic percent alloy concentration can reduce the drift mobility substantially. It can be seen that the rate of decrease near $x=0$ and $x=1$ are quite different. This is because the L edge has more s content than the X edge. Because the s

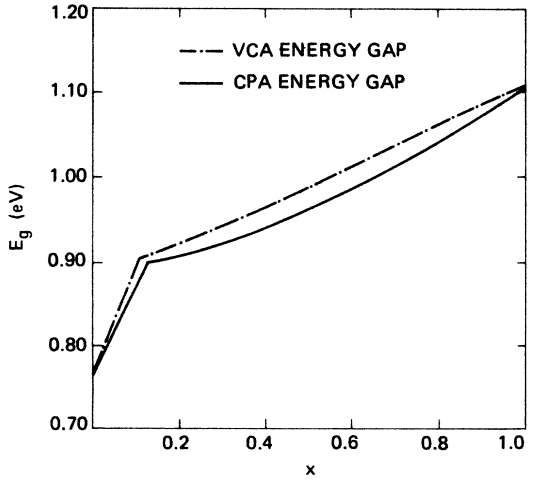

FIG. 6. Variation of the VCA energy gap (dash-dotted line) and the CPA energy gap (solid line) as a function of x.

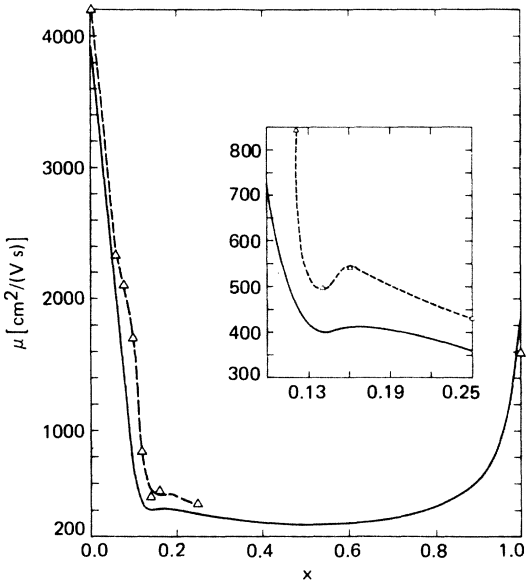

FIG. 7. Calculated drift mobility (solid line) and the experimental (dashed line) Hall mobility (Ref. 1) as a function of x.

scattering is dominant in these alloys, the L electrons are scattered more than the X electrons. Precisely for this reason, one observes a dip in the mobility near the L to X (Δ) crossover. For $x \lesssim 0.13$, the minimum gap is the L gap. After the crossover, the minimum gap is the X (Δ) gap, and the reduced alloy scattering increases the average mobility. For still larger x, the mobility decreases because of the increased alloy disorder. All these features are clearly seen in Fig. 7. While our calculations include the intervalley scattering mediated by alloy disorder, the effect of other scattering mechanisms is expected to increase the dip near the crossover.

The calculated alloy scattering rate for the holes is several orders smaller than that for electrons, because (1) the valence-band edge has dominant p content, (2) the p-scattering parameter ($\Delta\epsilon_p = 0.21$) is only $\frac{1}{7}$ of $\Delta\epsilon_s$, which alone decreases the scattering rate for holes by a factor of 50, and (3) finally, the imaginary part of the self-energy is proportional to the density of states, which approaches zero at the band edge. Hence, the hole mobility in this system is insensitive to alloy disorder.

In MCPA, the conduction band is pushed down, because of an increase in the imaginary part of the self-energy, giving rise to an additional bowing in the fundamental gap. For an $x = 0.50$ alloy, the gap is reduced by 7 meV. The bowing parameter, including the MCPA correction, is 0.21, which is in excellent agreement with experiment.[37]

It is interesting to compare the results of our calculations with those of Hass *et al.*[34] In their calculations on the $Ga_{1-x}In_xAs$ alloy, CPA introduced an extra bowing in the fundamental gap. However, after the MCPA corrections, the total scattering was diminished and the results were similar to VCA results. These results were explained in terms of the relative strength and sign of the atomic term values and V_2^{AB}. We extend their argument to Si_xGe_{1-x} alloys. The hybrid level of silicon is higher than that of germanium. Because of its shorter bond length, the V_2 of silicon is larger than that of germanium. Thus, in this case, both effects combine to give more disorder in the conduction and valence bands. Therefore, the scattering is enhanced in these alloys. This explains the increase in the imaginary part of the self-energy due to inclusion of OD disorder in our calculation.

In conclusion, we have incorporated both chemical and structural disorder into the calculation of the CPA band structure of Si_xGe_{1-x} alloys. The calculation, based on a realistic band structure of silicon and germanium, suggests that the band gap is an increasing function of x with a slope discontinuity at $x \simeq 0.13$. The linewidths of the E_0 and E_1 transitions calculated by CPA and MCPA are in good agreement with experiments. The effects of structural disorder on diagonal CPA for the Ge-Si alloy system will be difficult to test experimentally. MCPA decreases the band gap only slightly. However, unlike the GaInAs case, the imaginary part of the s self-energy increases with increasing energy and serves as a warning that all systems will not exhibit the same behavior. Therefore, in Ge-Si alloys, the place to look for experimentally significant differences between CPA and MCPA predictions is in the high-lying transitions. However, even in the E_0 transition, the MCPA linewidth at $x = 0.5$ is still only 10% larger than the corresponding CPA value. The calculated alloy-scattering-limited electron-drift mobility is in qualitative agreement with the observed Hall mobilities.

ACKNOWLEDGMENTS

This work was supported in part by U.S. Air Force Office of Scientific Research Grant No. AFOSR-84-0282 and Defense Advanced Research Projects Agency (DARPA)/AFOSR Project No. PR:FQ8671-851100. One of us (A.-B.C.) would like to thank Professor W. E. Spicer for his hospitality at Stanford University.

[1]M. Glicksman, Phys. Rev. **111**, 125 (1958); **100**, 1146 (1955).
[2]B. A. Bunker, S. L. Hulbert, J. P. Stotl, and F. C. Brown, Phys. Rev. Lett. **53**, 2157 (1984).
[3]H. J. Lee, L. Y. Juravel, and J. C. Woolley, Phys. Rev. B **21**, 659 (1980).
[4]N. Lifshitz, A. Jayaraman, and R. A. Logan, Phys. Rev. B **21**, 670 (1980).
[5]H. M. Manasevit, I. S. Gergis, and A. B. Jones, Appl. Phys. Lett. **41**, 464 (1982); J. Electron. Mater. **12**, 637 (1983).
[6]S. Krishnamurthy and J. A. Moriarty, Superlat. Microstruct. **1**, 209 (1985); Phys. Rev. B **32**, 1027 (1985).
[7]J. C. Bean, L. C. Feldman, A. T. Flory, S. Nakahara, and I. K. Robinson, J. Vac. Sci. Technol. A **2**, 436 (1984).
[8]R. People, J. C. Bean, D. V. Lang, A. M. Sergent, H. L. Storm-

er, K. W. Wecht, R. T. Lynch, and K. Baldwin, Appl. Phys. Lett. **45**, 1231 (1984).
[9]F. Cerdeira, A. Pinczuk, and J. C. Bean, Phys. Rev. B **31**, 1202 (1985).
[10]T. P. Pearsall, F. H. Pollak, and J. C. Bean, Bull. Am. Phys. Soc. **30**, 266 (1985).
[11]K. E. Newman and J. D. Dow, Phys. Rev. B **30**, 1929 (1984).
[12]M. Z. Huang and W. Y. Ching, Superlat. Microstruct. **1**, 137 (1985).
[13]D. Stroud and H. Ehrenreich, Phys. Rev. B **2**, 3197 (1970).
[14]S. Krishnamurthy, A. Sher, and A.-B. Chen, Phys. Rev. Lett. **55**, 320 (1985).
[15]S. Krishnamurthy, A. Sher, and A.-B. Chen, Appl. Phys. Lett. **47**, 160 (1985).
[16]A.-B. Chen and A. Sher, Phys. Rev. B **22**, 3886 (1980).
[17]E. O. Kane, Phys. Rev. B **13**, 3478 (1976).
[18]D. J. Chadi, Phys. Rev. B **16**, 3572 (1977).
[19]A.-B. Chen and A. Sher, Phys. Rev. B **23**, 5360 (1981).
[20]A.-B. Chen and A. Sher, Phys. Rev. B **26**, 6603 (1982).
[21]R. R. L. Zucca, J. P. Walter, Y. R. Shen, and M. L. Cohen, Solid State Commun. **8**, 627 (1970).
[22]R. R. L. Zucca and Y. R. Shen, Phys. Rev. B **1**, 2668 (1970).
[23]M. Welkowsky and R. Braunstein, Phys. Rev. B **5**, 497 (1972).
[24]R. A. Pollak, L. Ley, S. Kowalcyzk, D. A. Shirley, J. Joannopolos, D. J. Chadi, and M. L. Cohen, Phys. Rev. Lett. **29**, 1103 (1973).
[25]L. Ley, R. A. Pollak, F. R. McFeely, S. P. Kowalcyzk, and D. A. Shirley, Phys. Rev. B **9**, 600 (1974).
[26]W. D. Grobman and D. E. Eastman, Phys. Rev. Lett. **29**, 1508 (1972).
[27]D. E. Eastman, W. D. Grobman, J. L. Freeouf, and M. Erbudak, Phys. Rev. B **9**, 3473 (1974).
[28]W. E. Spicer and R. C. Eden, *Proceedings of the Ninth International Conference on the Physics of Semiconductors, 1968* (Nauka, Leningrad, 1969), Vol. 1, p. 61.
[29]G. W. Gobeli and F. G. Allen, Phys. Rev. **245**, A137 (1965).
[30]J. R. Cheliskowsky and M. L. Cohen, Phys. Rev. B **14**, 556 (1976), and references therein.
[31]J. A. Moriarty and S. Krishnamurthy, J. Appl. Phys. **54**, 1892 (1983).
[32]K. C. Hass, B. Velicky, and H. Ehrenreich, Phys. Rev. B **29**, 3697 (1984).
[33]F. Ducastelle, J. Phys. C **7**, 1795 (1974).
[34]K. C. Hass, R. J. Lampert, and H. Ehrenreich, Phys. Rev. Lett. **52**, 77 (1984).
[35]W. A. Harrison, *Electronic Structure and the Properties of Solids* (Freeman, San Francisco, 1980), p. 65.
[36]J. S. Kline, F. H. Pollak, and M. Cardona, Helv. Phys. Acta **41**, 968 (1968).
[37]R. Braunstein, A. R. Moore, and F. Herman, Phys. Rev. **109**, 695 (1958).